Results in Physics 8 (2018) 628–632

Contents lists available at ScienceDirect

Results in Physics

journal homepage: www.journals.elsevier.com/results-in-physics

The effects of the impurity distribution on the electrical and optical properties of Cr^{2+}:ZnSe nanowires: First-principles study

Shenyu Dai [a], Guoying Feng [a,*], Yuqin Zhang [a], Lijuan Deng [a], Hong Zhang [a], Shouhuan Zhou [a,b]

[a] College of Electronics & Information Engineering, Sichuan University, No. 24 South Section 1, Yihuan Road, Chengdu, Sichuan 610064, China
[b] North China Research Institute of Electro-Optics, Beijing 100015, China

ARTICLE INFO

Article history:
Received 6 November 2017
Received in revised form 18 December 2017
Accepted 30 December 2017
Available online 4 January 2018

Keywords:
First-principles
Nanowires
Impurity distribution
Cr-doped ZnSe

ABSTRACT

The structural, electrical and mid-infrared optical properties of wurtzite structured ZnSe nanowires with different Chromium impurity distribution are investigated using first-principles calculation based on density-functional theory (DFT). The formation energies have been calculated to study the relative stabilities of different Cr doping positions. It is shown that when the Cr doping position shifted from the center to the edge, the splitting energy between $^5T_2$ and ^5E levels of Cr d-orbitals is decreased and a redshift is observed in the calculated infrared absorption spectra. A probable reason for these effects of the impurity distribution is discussed.

Introduction

Semiconductor nanowires (NWs) have attracted considerable attention due to their unique optical, electronic and mechanical properties and their potential application in novel electronic and photonic devices [1–3]. Compared with their bulk counterpart, the bandgap of NWs is increased because of the quantum confinement effect. To test and understand the fundamental concepts about the roles of dimensionality and size on physical properties, much effort has been made to rationally synthesis semiconductor NWs in single crystal forms, with control of chemical composition, diameter, length, doping and electronic properties [4]. At present, semiconductor NWs represent one of the best-defined classes of nanoscale building blocks for nanoscience and nanotechnology [5].

Divalent transition metal ions (TM^{2+}) doped II-VI semiconductors are considered as promising laser gain media and optoelectronic materials in mid-infrared (MIR) region owing to their desirable qualities such as large absorption and emission bandwidth, large emission cross sections and low energy optical phonon cut-off [6]. Cr doped ZnSe is one of the most important member of these materials and has been demonstrated covering a broad range of regimes of operation and output parameters [7–12]. In our previous work, nanocrystalline Cr doped ZnSe NWs have been successfully fabricated for the first time, and shows strong emission at around 2000–2500 nm under excitation of 1300–2250 nm wavelength at room temperature [13]. Compared with their bulk counterpart, 1D nanostructure lasers have a lower threshold [14] and a shift in wavelength [13].

Although bulk ZnSe crystals have a stable zincblende crystal structure, experiments have proved that ZnSe nanowires can be synthesized in both cubic zincblende and hexagonal wurtzite structures [15–17]. Using an empirical interatomic potential approach which incorporates the electrostatic interaction between bond charges and that between ionic charges [18], Akiyama et al. have clarified the structural trends of ZnSe/ZnS NWs [19]. They found that the wurtzite structure is stabilized for ZnSe NWs with diameter less than 4 nm. Similar conclusion was obtained by Shi et al. with first-principles approaches [20].

In this article, first-principles studies of wurtzite structured ZnSe NWs with different Cr doping positions are performed to investigate the effects of the impurity distribution on the stability, electrical structures and mid-infrared optical properties. It is found that Cr atoms prefer to occupy the inner sites of the bare ZnSe nanowire. A redshift of the absorption coefficient in the mid-infrared region is observed as the doping position shift from the center to the edge of the NW. We expect that this work will extend *ab initio* studies in areas of mid-infrared nanomaterial laser.

Method of calculations

The first-principles calculation based on density-functional theory (DFT) was performed as implemented in the Vienna *ab initio* simulation package (VASP) [21] using the projector augmented wave (PAW) method [22]. The generalized gradient approximation

* Corresponding author.
E-mail address: guoing_feng@scu.edu.cn (G. Feng).

https://doi.org/10.1016/j.rinp.2017.12.075
2211-3797/

(GGA) of Perdew-Burke-Ernzerhof (PBE) functional [23] was used to evaluated the non-local exchange-correlation energy, with a planewave energy cutoff of 500 eV. A $1 \times 1 \times 4$ Monkhorst-Pack mesh was used for k-point sampling for atomic force relaxation, whereas a dense $1 \times 1 \times 8$ k-point mesh was used for computation of the total energy, electronic, and optical properties. The energy and force convergence criteria were 10^{-4} eV and 10^{-2} eV/Å, respectively. The valence electron configurations which included Zn ($3d^{10}4s^2$), Se ($4s^24p^4$) and Cr ($3d^54s^1$) were considered.

The calculated bulk lattice parameters of wurtzite structured ZnSe are $a = b = 4.005$, $c = 6.657$, slightly larger than the experimental value of $a = b = 3.974$, $c = 6.506$ [24]. The GGA-PBE calculation shows a direct band gap of 1.15 eV at G-point for bulk ZnSe, which is close to previous GGA result but lower than the experimental value of 2.67 eV. This underestimate in band gap calculation is due to the intrinsic shortcoming of DFT method. Some recently developed post-DFT method like DFT+U, HSE and GW can provide more accurate prediction of band gap, but they are also much more expensive than the ordinary GGA method. It is worth noting that in this article we mainly focus on the optical properties in the mid-infrared spectral region, which are resulted from the electron transitions between the impurity bands. The underestimate in band gaps will not affect the results and the GGA with PBE functional is sufficient, which have been verified by our previous theoretical and experimental works [25,26].

A wurtzite structured ZnSe nanowire (NW) along the [0001] direction with a diameter of about 2 nm is considered in this study, as shown in Fig. 1. The pristine ZnSe NW model is formed by 108 Zn and 108 Se atoms and is devised by cutting out a fragment from a $9 \times 9 \times 2$ bulk ZnSe supercells. The vacuum region is more than 10 Å, which is sufficiently large to reduce the interactions between adjacent NWs. In view of the fact that NWs are mainly fabricated by CVD methods in vacuum, the edge of the NW model are not terminated by any functional group. The Cr^{2+}-doped NWs are constructed by substituting a Zn atom in the unit cell of the pristine NW model with a Cr atom, and have a Cr^{2+} concentration of 0.93%. We choose five nonequivalent Zn positions from the center to the edge, labeled as p-1–p-5 (as shown in Fig. 1a), to study the influence of different doping sites.

Results and discussion

Fig. 2a shows the geometry of ZnSe NW after fully relaxation. From the optimized NW structures, we can find that the positions of the internal atoms approximately remain unchanged but atoms in the surface are significantly relaxed. The Zn atoms in the surface relax inward toward the bulk from their bulk-terminated position, while Se atoms slightly relax outward. Finally, the Zn atom lies in a plane with its three Se neighbors, effectively rehybridizing from sp^3 to sp^2. This surface dimer relaxation reflected that ZnSe is dominated by covalent character [27], similar to other II-VI materials [28]. Because the radius of the Cr atom is close to Zn atom, the optimized Cr^{2+}:ZnSe NWs structures are similar to the pristine ZnSe NW. In Fig. 2b, we plot the coordination structures of Cr atoms in five configurations of Cr^{2+}:ZnSe NWs. The Cr atoms and their nearby Se atoms have a tiny distortion. The average Cr-Se bond length for p-1–p-5 is 2.477 Å, 2.478 Å, 2.495 Å, 2.501 Å and 2.398 Å, respectively, which is slightly increased from the center to the edge, except for outermost position p-5. Same as ZnSe NW, Cr atom at surface position rehybridizing to sp^2 after geometry relaxation and no longer in tetrahedral symmetry.

To compare the relative stabilities of different doping positions, the formation energy of Cr^{2+}-doped nanowire was calculated by the following formula [29]:

$$E_{form} = E_{doped} - E_{pure} + \mu_{Zn} - \mu_{Cr} \quad (1)$$

where E_{pure} is the total energy of pristine pure ZnSe NW unit cell, E_{doped} is the total energy of Cr^{2+}-doped NW unit cell. μ_{Zn} and μ_{Cr} are the chemical potentials of Zn and Cr, respectively. The relations between μ_{Se} and the other atoms are as follows:

$$\mu_{Zn} + \mu_{Se} = \mu(\mathrm{ZnSe}) \quad (2)$$

$$\mu_{Cr} + \mu_{Se} = \mu(\mathrm{CrSe}) \quad (3)$$

The chemical potential can be changed from Se-rich to Zn-rich which depends on the growth condition. However, in this case, $\mu_{Zn} - \mu_{Cr}$ equals to $\mu(\mathrm{ZnSe}) - \mu(\mathrm{CrSe})$ and is a constant. It should be mentioned that the formation energy of Cr^{2+}-doped ZnSe bulk calculated from above formula is positive (~1.5 eV), indicating that it is hard to incorporate Cr into ZnSe crystals, which agrees with the experimental results. The Cr^{2+} concentration in a typical high doped Cr:ZnSe crystal fabricated by thermal diffusion method is usually with an order of magnitude of 10^{19} ions/cm^3, and the mass fraction is lower than 0.1% [30]. Fig. 3 shows the formation energies of different Cr doping positions in the NW. It is noted that the formation energies of Cr doped NWs are bigger than that of bulk, even for the lowest position p-2 (~1.8 eV). The results show that it is even harder to incorporate Cr into ZnSe NWs, however,

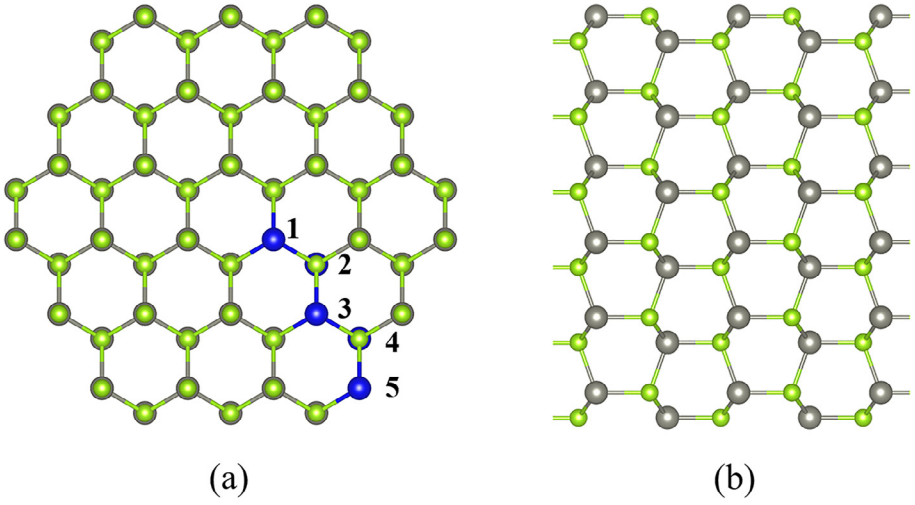

Fig. 1. Top (a) and side (b) views of a ZnSe NW model. Green and grey balls denote Se and Zn atoms, respectively. Blue balls numbered 1–5 denote the chosen nonequivalent Zn positions p-1–p-5. (For interpretation of the references to colour in this figure legend, the reader is referred to the web version of this article.)

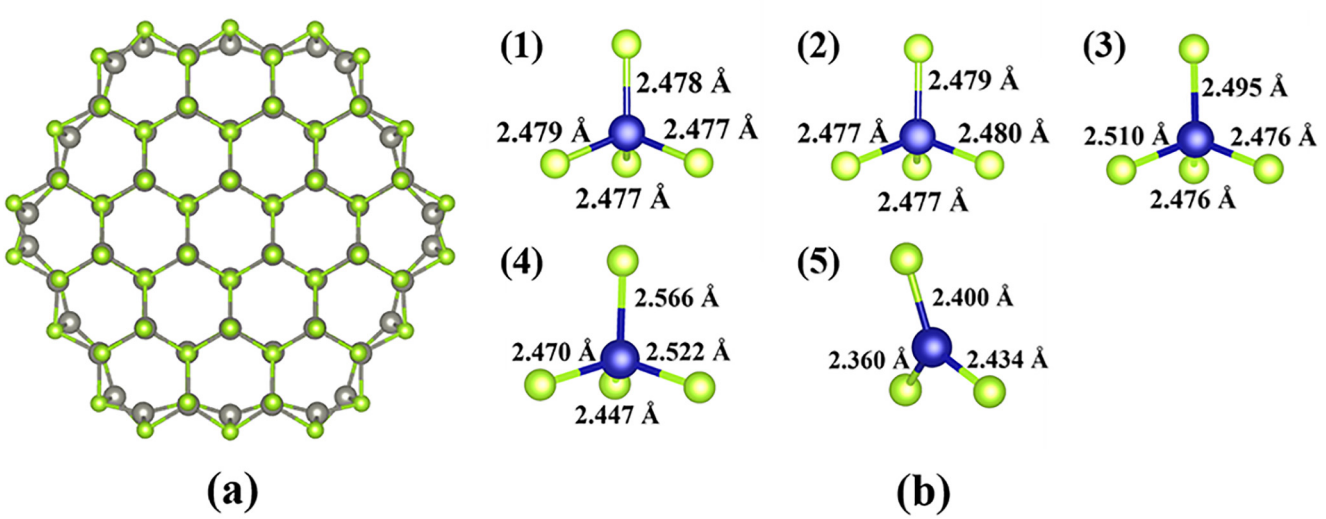

Fig. 2. (a) Top view of pristine ZnSe NW after relaxation. (b) Coordination structures of Cr atoms in 5 configurations of optimized Cr^{2+}:ZnSe NW models. Green, grey and blue ball are Se, Zn and Cr atoms, respectively. (For interpretation of the references to colour in this figure legend, the reader is referred to the web version of this article.)

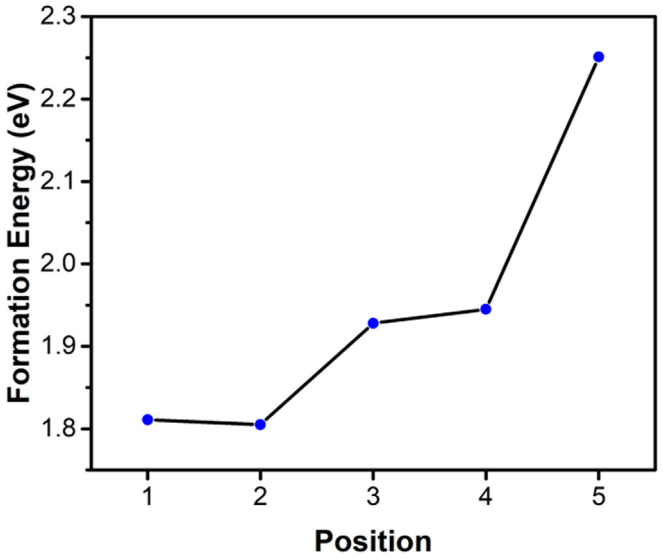

Fig. 3. The formation energies of Cr-doped ZnSe nanowires with different dopant positions.

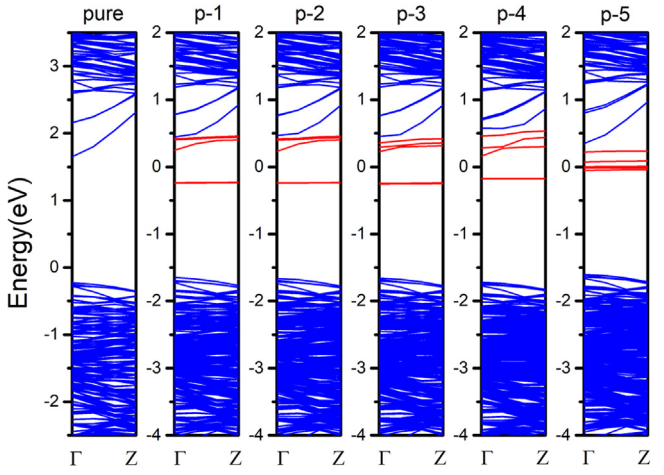

Fig. 4. Band structures of pure and Cr^{2+}-doped NWs. The red bands located at the bandgap corresponding to Cr impurity bands. The fermi levels have been chosen as zero of energy. (For interpretation of the references to colour in this figure legend, the reader is referred to the web version of this article.)

Cr^{2+} doped NWs can be made from pre-prepared Cr:ZnSe crystals [13] and the models are reasonable. From Fig. 3, we can find that the formation energy shows an upward trend when substituted Cr atom positions shift from the center to the edge and is significantly increased at the outermost site (p-5), indicating that Cr atoms prefer to occupy the inner sites of the ZnSe nanowires. The discrepancy of formation energies for different doping positions can be attributed to the change in bond lengths and the chemical environment when the host Zn atom is substituted by a Cr atom.

To investigate the influence of the Cr dopants and their doping positions on the modification of the electronic structures, the band structures and density of states (DOS) were calculated. Fig. 4 displays calculated band structures of pure and Cr^{2+}-doped NWs. The fermi levels (EFL) have been chosen as zero of energy. From the band structure, the conduction band minimum (CBM) and the valence band maximum (VBM) are both located at Γ point. The band gap energy of the pure NW is 1.880 eV, larger than that of bulk ZnSe calculated under the same conditions (1.15 eV). The bandgap value is reduced due to the well-known quantum confinement effect.

When Cr atoms enter a ZnSe crystal as impurities, they lose the electron of the 4 s shell and an electron of the 3d shell. The partly empty 3d shell is then the outermost shell and is strongly exposed to the action of the neighboring ions. The tetrahedral crystal field (T_d) of the surrounding ions splits fivefold degenerate ^5D ground state of free Cr^{2+} ions into triplet $^5T_2$ and duplet ^5E. The duplet ^5E is then the ground state of the substituted Cr^{2+} ions. The Energy splitting between $^5T_2$ and ^5E levels corresponds to the infrared spectral range and leads to infrared absorption and luminescence of Cr^{2+}-doped ZnSe materials. From the Fig. 4, there are five impurity bands (IB) appear in the bandgap (red bands in Fig. 4) of each Cr^{2+}-doped NW. The fermi levels shift upward, dividing the IBs into two group, indicating that these bands are partially occupied. For p-1–p-4, the substituted Cr^{2+} ions are in the tetrahedral crystal fields, and these two groups of IBs can correspond to $^5T_2$ and ^5E levels, respectively. But for p-5, the substituted Cr atom is in a

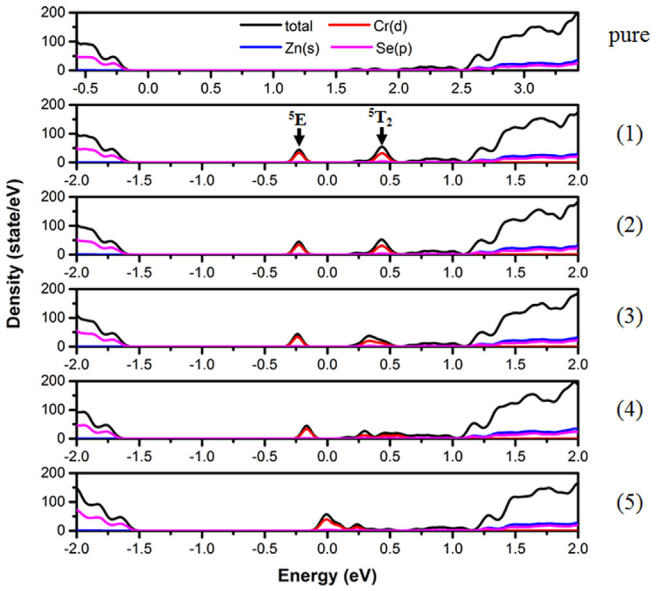

Fig. 5. DOS and PDOS for ZnSe NW and Cr^{2+}:ZnSe NWs.

trigonal field so the splitting levels are quite different. As the doping positions shift from the center to the edge, the splitting energy value between $^5T_2$ and ^5E levels is slightly reduced when the doping at inner sites, but greatly changes when Cr atom doping at surface.

Fig. 5 displays the total density of states (DOS) and partial density of states (PDOS) near the Fermi energy of ZnSe NW and Cr^{2+}:ZnSe NWs. We can find that the valence band edge is mainly formed by Se-p orbitals and the conduction band edge is mainly formed by Se-p and Zn-s orbitals, which are consistent with the bulk material. And as expected, the IBs are mainly derived from the d orbitals of Cr atoms and are separated into two peaks on the both side of the Fermi energy. As the doping sites of Cr atom move from the center to the edge, the splitting energy value between peak positions of $^5T_2$ and ^5E is reduced, which are 0.66, 0.65, 0.57, 0.45 and 0.25 eV for p-1–p-5 sites, respectively. This reduction in splitting energy is due to the distortion of the cage-like structure around the Cr atoms after relaxation. The average Cr-Se bond lengths are slightly increased when the doping sites shift from the center to the edge, leading to the weakening of the crystal field.

The optical properties of the Cr^{2+}-doped ZnSe nanowires are discussed based on the dielectric function and the absorption coefficient. The imaginary part ε_2 of the frequency dependent dielectric function $\varepsilon(\omega) = \varepsilon_1(\omega) + i\varepsilon_2(\omega)$ can be obtained after ground state calculation. Using Kramer-Kronig relations, the real part ε_1 can be evaluated from ε_2. The absorption coefficient can be calculated by the following formula,

$$\alpha(\omega) = \frac{\sqrt{2}\omega}{c}\left[(\varepsilon_1^2 + \varepsilon_2^2)^{1/2} + \varepsilon_1\right]^{1/2}$$

where ω is the frequency; c is the speed of light in vacuum.

The calculated imaginary part (ε_2) of dielectric functions for the ZnSe NW and Cr^{2+}:ZnSe NWs are shown in Fig. 6a. We can find that in high energy range the line shapes of for all NWs are almost the same, while the low energy range (<1 eV) of the ε_2 are quite different. An enlarged view of the energy from 0 to 1.8 eV are shown in the Fig. 6b. For Cr^{2+}:ZnSe NWs there are additional peaks appear in the low-energy region. In our previous works, it has been confirmed that these small peaks are derived from the impurity Cr^{2+} 3d states and is responsible for the infrared optical properties. From postion-1 to 4, the additional peak positions decrease from 0.66, 0.65, 0.57 to 0.45, consistent with the reduced splitting energy value between $^5T_2$ and ^5E levels calculated before. Similarly, the Cr doped at postion-5 is quite different with other positions which are in the tetrahedral crystal field.

The calculated absorption coefficients α of pure ZnSe NW and Cr^{2+}:ZnSe NWs with 4-coordinated doping positions are plotted in Fig. 7a. After Cr doping, an additional absorption peak appears in the infrared range compared with pure NW. In Fig. 7b, $\alpha_{doped} - \alpha_{pure}$ are plotted to investigate the effect of Cr doping on the absorption spectrum. We can find that as the doping site shift from the center to the edge, the absorption peak position shift to a longer wavelength. Calculated absorption peak for p-1–p-4 is located at 1851, 1854, 2172 and 2606 nm, respectively. The red-shift of the absorption peak position can be attributed to the weakening influence of external atoms as the doping sites shift to outside positions. The result shows Cr doped ZnSe NW can be used in infrared photoelectric devices.

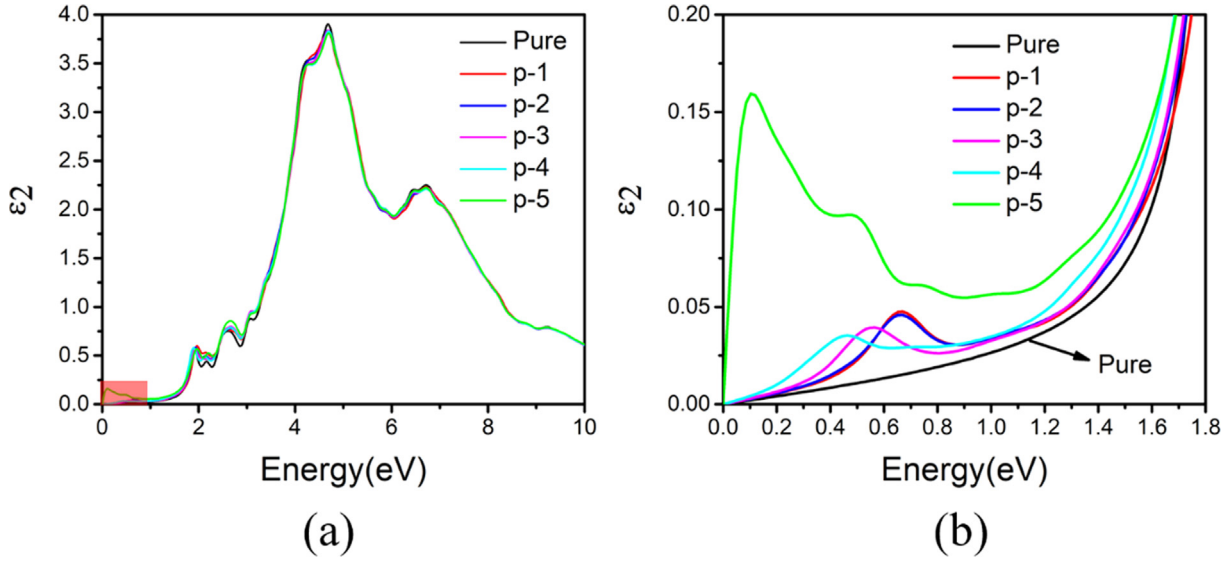

Fig. 6. (a) The calculated imaginary part ε_2 of pure ZnSe NW and Cr^{2+}:ZnSe NWs with different doping sites. (b) An enlarged image of the low energy region (red frame in (a)). (For interpretation of the references to colour in this figure legend, the reader is referred to the web version of this article.)

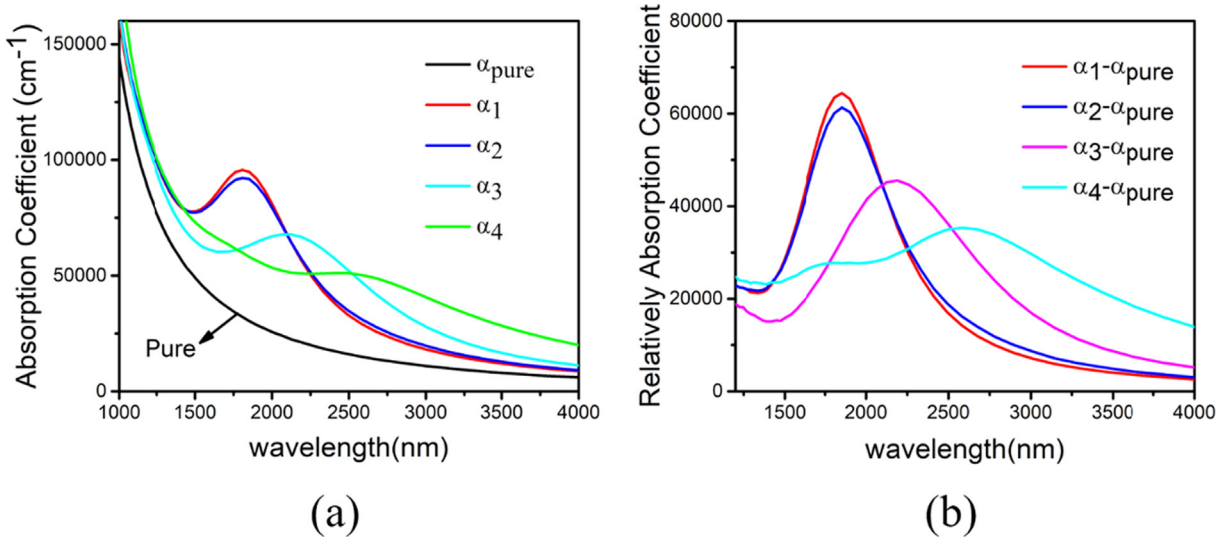

Fig. 7. (a) The calculated absorption coefficient and (b) $\alpha_{doped} - \alpha_{pure}$ as a function of wavelength for ZnSe NW and Cr^{2+}:ZnSe NWs with different doping positions.

Conclusion

In summary, the stability, electronic structures and mid-infrared optical properties of different Cr^{2+}-doped ZnSe nanowires are studied using density functional theory. It is found that Cr atoms prefer to occupy the inner sites of the bare ZnSe nanowire. The average Cr-Se bond length is slightly increased from the center to the edge. 5 impurity bands appear in the bandgap because of Cr doping, which are mainly derived from the d orbitals of Cr atoms. The Energy between the splitting $^5T_2$ and ^5E levels is responsible for the infrared optical properties of the material. As the doping positions shift from the center to the edge of the NWs, the splitting energy value is significantly reduced due to the Cr atom and its nearby Se atoms cage-like structure relaxation. A redshift of the absorption coefficient in the mid-infrared region is observed as the doping position shift from the center to the edge of the NW. The Cr^{2+}-Cr^{2+} interactions are not considered in present models and will be studied in further work. We expect that this work will extend *ab initio* studies in areas of mid-infrared nanomaterial laser.

Acknowledgments

This work was supported by the National Natural Science Foundation of China (NSFC No. 11574221).

References

[1] Jacobsson D et al. Interface dynamics and crystal phase switching in GaAs nanowires. Nature 2016;531(7594):317–22.
[2] Greytak AB et al. Semiconductor nanowire laser and nanowire waveguide electro-optic modulators. Appl Phys Lett 2005;87(15):151103.
[3] Chiesa M et al. Detection of the early stage of recombinational DNA repair by silicon nanowire transistors. Nano Lett 2012;12(3):1275–81.
[4] Agarwal R, Lieber CM. Semiconductor nanowires: optics and optoelectronics. Appl Phys A 2006;85(3):209.
[5] Wang ZL. Nanowires and nanobelts: materials, properties and devices. Volume 1: metal and semiconductor nanowires. Springer Science & Business Media; 2013.
[6] Mirov SB et al. Progress in Mid-IR lasers based on Cr and Fe-doped II-VI chalcogenides. IEEE J Sel Top Quantum Electron 2015;21(1):292–310.
[7] Macdonald JR et al. Efficient mid-infrared Cr: ZnSe channel waveguide laser operating at 2486 nm. Opt Lett 2013;38(13):2194–6.
[8] Moskalev I et al. 140 W Cr:ZnSe laser system. Opt Express 2016;24 (18):21090–104.
[9] Wang Z et al. Multi-layered black phosphorus as saturable absorber for pulsed Cr: ZnSe laser at 2.4 μm. Opt Express 2016;24(2):1598–603.
[10] Vasilyev S, Mirov M, Gapontsev V. Kerr-lens mode-locked femtosecond polycrystalline Cr 2+: ZnS and Cr 2+: ZnSe lasers. Opt Express 2014;22 (5):5118–23.
[11] Sorokin E, Sorokina IT. Tunable diode-pumped continuous-wave Cr 2+: ZnSe laser. Appl Phys Lett 2002;80(18):3289–91.
[12] Sorokina IT et al. Efficient broadly tunable continuous-wave Cr 2+: ZnSe laser. JOSA B 2001;18(7):926–30.
[13] Feng G, Yang C, Zhou S. Nanocrystalline Cr(2+)-doped ZnSe nanowires laser. Nano Lett 2013;13(1):272–5.
[14] Gradečak S et al. GaN nanowire lasers with low lasing thresholds. Appl Phys Lett 2005;87(17):173111.
[15] Shan CX et al. Wurtzite ZnSe nanowires: growth, photoluminescence, and single-wire Raman properties. Nanotechnology 2006;17(22):5561–4.
[16] Zannier V et al. Optical properties of single wurtzite/zinc-blende ZnSe nanowires grown at low temperature. J Appl Phys 2015;118(9):095702.
[17] Zhang Q et al. ZnSe nanostructures: Synthesis, properties and applications. Prog Mater Sci 2016;83:472–535.
[18] Akiyama T et al. An empirical potential approach to wurtzite–zinc-blende polytypism in group III–V semiconductor nanowires. Jpn J Appl Phys 2006;45 (3L):L275.
[19] Akiyama T et al. An empirical interatomic potential approach to structural stability of ZnS and ZnSe nanowires. Jpn J Appl Phys 2007;46(4R):1783.
[20] Chen H et al. The stability and electronic properties of wurtzite and zinc-blende ZnS nanowires. Phys Lett A 2009;373(3):371–5.
[21] Kresse G, Furthmüller J. Efficient iterative schemes for ab initio total-energy calculations using a plane-wave basis set. Phys Rev B 1996;54(16):11169–86.
[22] Kresse G, Joubert D. From ultrasoft pseudopotentials to the projector augmented-wave method. Phys Rev B 1999;59(3):1758–75.
[23] Perdew JP, Burke K, Ernzerhof M. Generalized gradient approximation made simple [Phys. Rev. Lett. 77, 3865 (1996)]. Phys Rev Lett 1997;78(7). 1396-1396.
[24] Yeh C-Y et al. Zinc-blende–wurtzite polytypism in semiconductors. Phys Rev B 1992;46(16):10086.
[25] Zhang Y et al. First-principles study of the electronic structures and optical properties of Cr^{2+}-doped ZnSe as a function of impurity concentration. Phys Status Solidi B 2016;253(6):1133–7.
[26] Zhang Y et al. Theoretical and experimental study of the absorption spectra of Cr2+: ZnS and Fe2+: ZnS. J Comput Theo Nanosci 2015;12(8):1956–8.
[27] Swarts CA, Goddard WA, McGill TC. *Theoretical studies of the reconstruction of the (110) surface of III–V and II–VI semiconductor compounds.* J Vac Sci Technol 1980;17(5):982–6.
[28] Bendavid LI, Carter EA. First principles study of bonding, adhesion, and electronic structure at the Cu2O(111)/ZnO interface. Surf Sci 2013;618:62–71.
[29] Long R, English NJ. Synergistic effects of Bi/S codoping on visible light-activated anatase TiO2 photocatalysts from first principles. J Phys Chem C 2009;113(19):8373–7.
[30] Demirbas U, Sennaroglu A, Somer M. Synthesis and characterization of diffusion-doped Cr2+:ZnSe and Fe2+:ZnSe. Opt Mater 2006;28(3):231–40.